BNL-225174-2024-TECH
EIC-ADD-TN-081

Generalized wakefield of a microbunched electron cooler

P. Baxevanis

December 2023

Electron-Ion Collider
Brookhaven National Laboratory

U.S. Department of Energy
USDOE Office of Science (SC), Nuclear Physics (NP)

DISCLAIMER

Generalized wakefield of a microbunched electron cooler

Panagiotis Baxevanis

I. INTRODUCTION

In a previous note [1] we developed theoretical and computational tools for the study of microbunched electron cooling (MBEC [2]) in the three-dimensional regime. In this context, we were able to treat the key space charge effect in a rigorous fashion by taking explicitly into account the point-charge nature of the particles involved (electrons and hadrons). In this report, we build upon our earlier analysis by taking into consideration previously neglected effects that can cause Landau damping in the amplifier section (such as focusing, betatron oscillations and the angular spread of the electron beam). Beginning with the theoretical aspect of this work, we use our modified and expanded tools in order to calculate and study the generalized, point-hadron wakefield of the system, an important quantity that affects the cooling performance.

II. THEORETICAL ANALYSIS

We start our analysis by revisiting the problem of plasma oscillations in a round electron beam of finite transverse size, but extend our treatment to the fully three-dimensional regime, including the effects of angular spread and focusing. Recalling the discussion of single particle dynamics in Ref. [1], the longitudinal portion of the equations of motion for a single electron may be written as

$$\frac{dz}{ds} = \frac{\eta}{\gamma_0^2} - \frac{1}{2}(p_x^2 + p_y^2 + k_\beta^2(x^2+y^2))\,, \tag{1}$$

$$\frac{d\eta}{ds} = \frac{e^2}{\gamma_0 m_e c^2}\int dx'dy'dz'\delta n(x',y',z';s)\Phi(x-x',y-y',z-z')\,, \tag{2}$$

where s is the longitudinal position in the lab frame, z is the internal beam coordinate, η is the energy deviation, δn is the electron beam volume density perturbation and $\Phi(x,y,z) = \gamma_0 z/(x^2+y^2+\gamma_0^2 z^2)^{3/2}$ is the scaled interaction function for the longitudinal space charge force. Moreover, γ_0 is the average relativistic factor of the beam, e and m_e are the charge and mass of the electrons (respectively), while k_β is the transverse focusing strength. The latter also determines the period of the (symmetric and smooth) betatron oscillations, which are described by

$$\frac{d\mathbf{x}}{ds} = \mathbf{p}\,,\, \frac{d\mathbf{p}}{ds} = -k_\beta^2\mathbf{x}\,, \tag{3}$$

where $\mathbf{x} = (x, y)$ is the transverse position vector and $\mathbf{p} = (p_x, p_y)$ is its momentum counterpart.

The generalized distribution function F for the electron beam can be decomposed as

$$F(\mathbf{x}, \mathbf{p}, z, \eta; s) = n_0 F_0(\mathbf{x}, \mathbf{p}, \eta) + \delta F(\mathbf{x}, \mathbf{p}, z, \eta; s)\,, \tag{4}$$

where n_0 is the background *line* density of the beam,

$$F_0 = \frac{1}{(2\pi)^{5/2}\Sigma_p^2\Sigma_p'^2\sigma_e} \exp(-\frac{\mathbf{p}^2 + k_\beta^2\mathbf{x}^2}{2\Sigma_p'^2}) \exp(-\frac{\eta^2}{2\sigma_e^2})\,, \tag{5}$$

(where Σ_p is the rms size of the round beam, $\Sigma_p' = k_\beta\Sigma_p$ is the corresponding angular spread and σ_e is the rms value of the energy spread) and δF is a small perturbation, which can be liked to δn via

$$\delta n(\mathbf{x}, z; s) = \int d^2\mathbf{p} d\eta \delta F(\mathbf{x}, \mathbf{p}, z, \eta; s)\,. \tag{6}$$

Here, we have tacitly assumed that the beam is matched to the focusing channel and thus has a constant (i.e. s-independent) transverse profile. It should also be noted that Σ_p and Σ_p' can be obtained from the transverse emittance ϵ via $\Sigma_p = (\epsilon\beta_p)^{1/2}$ and $\Sigma_p' = (\epsilon/\beta_p)^{1/2}$, where $\beta_p = 1/k_\beta$ is the matched electron beta function.

The self-consistent evolution of the electron beam distribution function is governed by the Vlasov equation, namely

$$\frac{\partial F}{\partial s} + \frac{d\mathbf{x}}{ds}\frac{\partial F}{\partial \mathbf{x}} + \frac{d\mathbf{p}}{ds}\frac{\partial F}{\partial \mathbf{p}} + \frac{dz}{ds}\frac{\partial F}{\partial z} + \frac{d\eta}{ds}\frac{\partial F}{\partial \eta} = 0\,, \tag{7}$$

the first-order (linearized) component of which can be written as

$$\frac{\partial(\delta F)}{\partial s} + \mathbf{p}\frac{\partial(\delta F)}{\partial \mathbf{x}} - k_\beta^2\mathbf{x}\frac{\partial(\delta F)}{\partial \mathbf{p}} + [\frac{\eta}{\gamma_0^2} - \frac{1}{2}(\mathbf{p}^2 + k_\beta^2\mathbf{x}^2)]\frac{\partial(\delta F)}{\partial z} + n_0\frac{e^2\mathcal{E}(\mathbf{x}, z; s)}{\gamma_0 m_e c^2}\frac{\partial F_0}{\partial \eta} = 0\,, \tag{8}$$

where

$$\mathcal{E}(\mathbf{x}, z; s) = \int d^2\mathbf{x}' dz' \delta n(\mathbf{x}', z'; s)\Phi(\mathbf{x} - \mathbf{x}', z - z')\,. \tag{9}$$

Introducing the Fourier quantities $\delta\hat{F}_z$ and $\hat{\mathcal{E}}_z$ via the definitions

$$\delta F(\mathbf{x}, \mathbf{p}, z, \eta; s) = \frac{1}{2\pi}\int dk_z \delta\hat{F}_z(\mathbf{x}, \mathbf{p}, k_z, \eta; s)\exp(ik_z z)\,, \tag{10}$$

$$\mathcal{E}(\mathbf{x}, z; s) = \frac{1}{2\pi}\int dk_z \hat{\mathcal{E}}_z(\mathbf{x}, k_z; s)\exp(ik_z z)\,, \tag{11}$$

the frequency-domain, linearized Vlasov equation becomes

$$\frac{\partial(\delta\hat{F}_z)}{\partial s} + \mathbf{p}\frac{\partial(\delta\hat{F}_z)}{\partial \mathbf{x}} - k_\beta^2\mathbf{x}\frac{\partial(\delta\hat{F}_z)}{\partial \mathbf{p}} + [\frac{\eta}{\gamma_0^2} - \frac{1}{2}(\mathbf{p}^2 + k_\beta^2\mathbf{x}^2)]ik_z\delta\hat{F}_z + n_0\frac{e^2\hat{\mathcal{E}}_z}{\gamma_0 m_e c^2}\frac{\partial F_0}{\partial \eta} = 0\,. \tag{12}$$

The partial differential equation given above can be solved using the method of integration along unperturbed trajectories. Its formal solution is

$$\delta\hat{F}_z(\mathbf{x},\mathbf{p},k_z,\eta;s) = \delta\hat{F}_z(\mathbf{x}_0,\mathbf{p}_0,k_z,\eta;0)\exp(-ik_z s[\eta/\gamma_0^2 - (\mathbf{p}^2+k_\beta^2\mathbf{x}^2)/2]) \\ - n_0\frac{e^2}{\gamma_0 m_e c^2}\frac{\partial F_0}{\partial\eta}\int_0^s ds'\hat{\mathcal{E}}_z(\mathbf{x}_+,k_z;s')\exp(ik_z(s'-s)[\eta/\gamma_0^2-(\mathbf{p}^2+k_\beta^2\mathbf{x}^2)/2])\,, \tag{13}$$

where

$$\mathbf{x}_+ = \mathbf{x}\cos(k_\beta(s'-s)) + \mathbf{p}\sin(k_\beta(s'-s))/k_\beta\,, \\ \mathbf{x}_0 = \mathbf{x}\cos(k_\beta s) - \mathbf{p}\sin(k_\beta s)/k_\beta\,, \\ \mathbf{p}_0 = k_\beta\mathbf{x}\sin(k_\beta s) + \mathbf{p}\cos(k_\beta s)\,. \tag{14}$$

As in our previous note, we remark that the above equations only contain the longitudinal wavenumber k_z. Next, we introduce the *full* Fourier space quantities $\delta\hat{F}_\mathbf{k}$ and $\hat{\mathcal{E}}_\mathbf{k}$ via

$$\delta\hat{F}_\mathbf{k} = \int d^2\mathbf{x}\exp(-i\mathbf{k}_\perp\cdot\mathbf{x})\delta\hat{F}_z = \int d^2\mathbf{x}dz\exp(-i\mathbf{k}_\perp\cdot\mathbf{x}-ik_z z)\delta F \tag{15}$$

and

$$\hat{\mathcal{E}}_\mathbf{k} = \int d^2\mathbf{x}\exp(-i\mathbf{k}_\perp\cdot\mathbf{x})\hat{\mathcal{E}}_z = \int d^2\mathbf{x}dz\exp(-i\mathbf{k}_\perp\cdot\mathbf{x}-ik_z z)\mathcal{E}\,, \tag{16}$$

where $\mathbf{k}_\perp = (k_x,k_y)$ is the transverse wavenumber vector. The corresponding Fourier transform of the density perturbation $\delta n(\mathbf{x},z)$ is defined by

$$\delta\hat{n}_\mathbf{k} = \int d^2\mathbf{x}dz\exp(-i\mathbf{k}_\perp\cdot\mathbf{x}-ik_z z)\delta n \tag{17}$$

and satisfies the relations

$$\delta\hat{n}_\mathbf{k} = \int d^2\mathbf{p}d\eta\delta\hat{F}_\mathbf{k} \tag{18}$$

and

$$\hat{\mathcal{E}}_\mathbf{k} = -\frac{4\pi i k_z\delta\hat{n}_\mathbf{k}}{k_z^2+\gamma_0^2(k_x^2+k_y^2)}\,. \tag{19}$$

Using all of the above, it again becomes straightforward to obtain a single equation for $\delta\hat{n}_\mathbf{k}$ (after some rather lengthy algebra). The end result of this manipulation is

$$\delta\hat{n}_\mathbf{k}(s) = \delta\hat{n}_\mathbf{k}^{(0)}(s) + \frac{e^2 n_0 k_z^2}{\pi\gamma_0^3 m_e c^2}\int_0^s ds'(s'-s)\frac{\exp(-\sigma_e^2 k_z^2(s'-s)^2/(2\gamma_0^4))}{(1+i\Sigma_p'^2 k_z(s'-s))^2} \\ \times\int d^2\mathbf{k}'_\perp\exp\left(-\frac{\Sigma_p^2}{2}\frac{\mathbf{k}_\perp^2+\mathbf{k}_\perp'^2-2\mathbf{k}_\perp\cdot\mathbf{k}'_\perp\cos(k_\beta(s'-s))}{1+i\Sigma_p'^2 k_z(s'-s)}\right)\frac{\delta\hat{n}_{\mathbf{k}'_\perp,k_z}(s')}{k_z^2+\gamma_0^2\mathbf{k}_\perp'^2}\,, \tag{20}$$

where

$$\delta\hat{n}_{\mathbf{k}}^{(0)}(s) = \int d^2\mathbf{x}d^2\mathbf{p}d\eta\delta\hat{F}_z(\mathbf{x}_0,\mathbf{p}_0,k_z,\eta;0)\exp(-ik_z s[\eta/\gamma_0^2-(\mathbf{p}^2+k_\beta^2\mathbf{x}^2)/2]-i\mathbf{k}_\perp\cdot\mathbf{x})\,, \quad (21)$$

is the evolution of $\delta\hat{n}_{\mathbf{k}}$ without the influence of longitudinal space charge. This integral equation can be solved numerically with the aid of a suitable routine for the fast calculation of 2D convolution integrals.

Next, we show how the result given above is modified by adding a chicane with strength R_{56} after a drift space of length L_d. Recalling (from [1]) that the Fourier component $\delta\hat{F}_{\mathbf{k}}$ is shifted according to

$$\delta\hat{F}_{\mathbf{k}} \to \delta\hat{F}_{\mathbf{k}}\exp(-ik_z R_{56}\eta)\,, \quad (22)$$

we combine this result with the derivation that led to Eq. (20), a manipulation which leads to the conclusion that the value of $\delta\hat{n}_{\mathbf{k}}$ after the chicane is expressed by

$$\begin{aligned}
\delta\hat{n}_{\mathbf{k}}^{+}(L_d) &= \int d^2\mathbf{x}d^2\mathbf{p}d\eta\exp(-i\eta k_z(L_d/\gamma_0^2+R_{56}))\delta\hat{F}_z(\mathbf{x}_0,\mathbf{p}_0,k_z,\eta;0)\\
&\times\exp(ik_z L_d(\mathbf{p}^2+k_\beta^2\mathbf{x}^2)/2-i\mathbf{k}_\perp\cdot\mathbf{x})\\
&+\frac{e^2 n_0 k_z^2}{\pi\gamma_0^3 m_e c^2}\int_0^{L_d} ds'(s'-L_d-\gamma_0^2 R_{56})\frac{\exp(-\sigma_e^2((s'-L_d)/\gamma_0^2-R_{56})^2k_z^2/2)}{(1+i\Sigma_p'^2k_z(s'-L_d))^2}\\
&\times\int d^2\mathbf{k}'_\perp\exp\left(-\frac{\Sigma_p^2}{2}\frac{\mathbf{k}_\perp^2+\mathbf{k}_\perp'^2-2\mathbf{k}_\perp\cdot\mathbf{k}'_\perp\cos(k_\beta(s'-L_d))}{1+i\Sigma_p'^2k_z(s'-L_d)}\right)\frac{\delta\hat{n}_{\mathbf{k}'_\perp,k_z}(s')}{k_z^2+\gamma_0^2\mathbf{k}_\perp'^2}\,. \quad (23)
\end{aligned}$$

In common with the analysis in our previous note, Eq. (23) is supposed to be used in conjunction with the numerical solution of Eqs. (20)-(21).

The results presented so far can be re-derived and generalized in the following way: a "thin" chicane of strength R_e (that is, a chicane with a length considerably smaller than the average electron beta function) is characterized by the simple transfer map $z_2 = z_1 + R_e\eta_1$, $\eta_2 = \eta_1$, the transverse phase space coordinates being unchanged. In order to incorporate this discrete jump into the "continuous" electron equations of motion, we need to rewrite Eq. (1) as

$$\frac{dz}{ds} = \frac{\eta}{\gamma_0^2} - \frac{1}{2}(p_x^2+p_y^2+k_\beta^2(x^2+y^2)) + R_e\eta\delta(s-s_e)\,, \quad (24)$$

where $s = s_e$ is the location of the chicane. In this way we emphasize that the amplification section contains two sources for R_{56}, a continuous one due to the drift ($\propto 1/\gamma^2$) and a discrete, localized counterpart due to the chicane. In view of this change, the solution to

the linearized, frequency-domain Vlasov equation becomes

$$\delta\hat{F}_z(\mathbf{x},\mathbf{p},k_z,\eta;s)=\delta\hat{F}_z(\mathbf{x}_0,\mathbf{p}_0,k_z,\eta;0)\exp(-ik_zs[\eta/\gamma_0^2-(\mathbf{p}^2+k_\beta^2\mathbf{x}^2)/2]-ik_zR_e\eta H(s-s_e))$$
$$-n_0\frac{e^2}{\gamma_0 m_e c^2}\frac{\partial F_0}{\partial\eta}\int_0^s ds'\hat{\mathcal{E}}_z(\mathbf{x}_+,k_z;s')\exp(ik_z(s'-s)[\eta/\gamma_0^2-(\mathbf{p}^2+k_\beta^2\mathbf{x}^2)/2]$$
$$+ik_zR_e\eta[H(s'-s_e)-H(s-s_e)])\,, \tag{25}$$

where $H(s)$ is the Heaviside step function (equal to 1 for $s>0$ and 0 for $s\leq 0$, for which we also have $H'(s)=\delta(s)$). Following the same procedure as before we find that the analogues to Eq. (20)-(21) are

$$\delta\hat{n}_{\mathbf{k}}(s)=\delta\hat{n}_{\mathbf{k}}^{(0)}(s)+\frac{e^2n_0k_z^2}{\pi\gamma_0m_ec^2}\int_0^s ds'((s'-s)/\gamma_0^2+R_e[H(s'-s_e)-H(s-s_e)])$$
$$\times\frac{\exp(-\sigma_e^2k_z^2((s'-s)/\gamma_0^2+R_e[H(s'-s_e)-H(s-s_e)])^2/2)}{(1+i\Sigma_p'^2k_z(s'-s))^2}$$
$$\times\int d^2\mathbf{k}'_\perp\exp\left(-\frac{\Sigma_p^2}{2}\frac{\mathbf{k}_\perp^2+\mathbf{k}_\perp'^2-2\mathbf{k}_\perp\cdot\mathbf{k}'_\perp\cos(k_\beta(s'-s))}{1+i\Sigma_p'^2k_z(s'-s)}\right)\frac{\delta\hat{n}_{\mathbf{k}'_\perp,k_z}(s')}{k_z^2+\gamma_0^2\mathbf{k}_\perp'^2}\,, \tag{26}$$

and

$$\delta\hat{n}_{\mathbf{k}}^{(0)}(s)=\int d^2\mathbf{x}d^2\mathbf{p}d\eta\delta\hat{F}_z(\mathbf{x}_0,\mathbf{p}_0,k_z,\eta;0)\exp(-ik_zs[\eta/\gamma_0^2-(\mathbf{p}^2+k_\beta^2\mathbf{x}^2)/2]$$
$$-ik_zR_e\eta H(s-s_e)-i\mathbf{k}_\perp\cdot\mathbf{x})\,, \tag{27}$$

respectively. By taking $s_e=L_d+0^+$ and $s=s_e+0^+$ we essentially recover Eq. (23) from the above expressions. Indeed, a very useful feature of Eqs. (26)-(27) is that they can be easily generalized to the case of *multiple* chicanes separated by drifts, thus covering the configuration of a multi-stage amplifier (of course, one has to assume symmetric smooth focusing with strength k_β for all the drifts, which is typically the case). In particular, for a collection of chicanes with strengths $R_{e,i}$ located at $s=s_{e,i}$ the phase equation becomes

$$\frac{dz}{ds}=\frac{\eta}{\gamma_0^2}-\frac{1}{2}(p_x^2+p_y^2+k_\beta^2(x^2+y^2))+\eta\sum_i R_{e,i}\delta(s-s_{e,i})\,, \tag{28}$$

and the propagation of the electron beam microbunching is accordingly governed by

$$\delta\hat{n}_{\mathbf{k}}(s)=\delta\hat{n}_{\mathbf{k}}^{(0)}(s)+\frac{e^2n_0k_z^2}{\pi\gamma_0m_ec^2}\int_0^s ds'((s'-s)/\gamma_0^2+\sum_i R_{e,i}[H(s'-s_{e,i})-H(s-s_{e,i})])$$
$$\times\frac{\exp(-\sigma_e^2k_z^2((s'-s)/\gamma_0^2+\sum_i R_{e,i}[H(s'-s_{e,i})-H(s-s_{e,i})])^2/2)}{(1+i\Sigma_p'^2k_z(s'-s))^2}$$
$$\times\int d^2\mathbf{k}'_\perp\exp\left(-\frac{\Sigma_p^2}{2}\frac{\mathbf{k}_\perp^2+\mathbf{k}_\perp'^2-2\mathbf{k}_\perp\cdot\mathbf{k}'_\perp\cos(k_\beta(s'-s))}{1+i\Sigma_p'^2k_z(s'-s)}\right)\frac{\delta\hat{n}_{\mathbf{k}'_\perp,k_z}(s')}{k_z^2+\gamma_0^2\mathbf{k}_\perp'^2}\,, \tag{29}$$

and

$$\delta\hat{n}_{\mathbf{k}}^{(0)}(s) = \int d^2\mathbf{x}d^2\mathbf{p}d\eta\delta\hat{F}_z(\mathbf{x}_0,\mathbf{p}_0,k_z,\eta;0)\exp(-ik_z s[\eta/\gamma_0^2-(\mathbf{p}^2+k_\beta^2\mathbf{x}^2)/2] \\ -ik_z\eta\sum_i R_{e,i}H(s-s_{e,i})-i\mathbf{k}_\perp\cdot\mathbf{x})\,. \tag{30}$$

Through this formalism, the analysis of the standard two-stage configuration for the amplifier section is no more complicated than its single-stage counterpart.

So far our treatment has focused on the propagation of electron density perturbations through the amplification cascade alone. In what follows, we outline how the same methodology can be used to describe the entire electron portion of the cooling lattice (from the start of the modulator to the end of the kicker). To begin with, we now assume that the smooth focusing approximation for the betatron oscillations applies to all modules of the system (modulator, amplifier and kicker sections), with beta functions that are constant within each segment but (in general) different in x and y. Even though this deviation from symmetry is introduced primarily in order to account for typical configurations of the electron beam in the modulator and kicker (themselves driven by the non-round hadron beam), the resulting formalism can deal with asymmetric focusing in the amplifier as well. As was discussed in our first note (in the context of describing the simulation algorithm), the short transition elements between the modules are modeled by simple maps that preserve the transverse emittance. In this expanded model, the electron betatron oscillations are governed by

$$\frac{dx}{ds}=p_x\,,\frac{dy}{ds}=p_y\,,\frac{dp_x}{ds}=-\frac{x}{\beta_x^2(s)}\,,\frac{dp_y}{ds}=-\frac{y}{\beta_y^2(s)}\,, \tag{31}$$

where $\beta_{x,y}(s)$ are the *piecewise-constant* electron beta functions. On the other hand, the equilibrium distribution for the matched electron beam can be written as

$$F_0=\frac{1}{(2\pi)^{5/2}\Sigma_x\Sigma_y\Sigma'_x\Sigma'_y\sigma_e}\exp(-\frac{x^2}{2\Sigma_x^2}-\frac{p_x^2}{2\Sigma_x'^2})\exp(-\frac{y^2}{2\Sigma_y^2}-\frac{p_y^2}{2\Sigma_y'^2})\exp(-\frac{\eta^2}{2\sigma_e^2})\,. \tag{32}$$

Here, the rms beam sizes $\Sigma_{x,y}$ and angular spreads $\Sigma'_{x,y}$ (both sets of quantities now s-dependent in a piecewise-constant fashion) are respectively given by $\Sigma_{x,y}(s)=(\epsilon_{x,y}\beta_{x,y}(s))^{1/2}$ and $\Sigma'_{x,y}(s)=(\epsilon_{x,y}/\beta_{x,y}(s))^{1/2}$, where $\epsilon_{x,y}$ are the electron transverse emittances (for typical parameters, we have $\epsilon_x=\epsilon_y=\epsilon$). As far as the phase equation is concerned, its final (continuous) form is

$$\frac{dz}{ds}=\frac{\eta}{\gamma_0^2}-\frac{1}{2}\{p_x^2+p_y^2+\frac{x^2}{\beta_x^2(s)}+\frac{y^2}{\beta_y^2(s)}\}+\eta\sum_i R_{e,i}\delta(s-s_{e,i})\,, \tag{33}$$

where the sum now also includes the contribution of the first chicane (immediately after the modulator). To complete our unified treatment of the cooling lattice, we need to incorporate the interactions associated with the hadrons in the modulator and kicker segments. In particular, owing to the presence of the hadron beam in the aforementioned modules, the energy equation for a test electron is modified according to

$$\begin{aligned}\frac{d\eta}{ds} =& \frac{e^2}{\gamma_0 m_e c^2}\int dx'dy'dz'\delta n(x',y',z';s)\Phi(x-x',y-y',z-z') \\ &- \frac{Ze^2}{\gamma_0 m_e c^2}\int dx'dy'dz'\delta n^{(h)}(x',y',z';s)\Phi(x-x',y-y',z-z')\,, \end{aligned} \tag{34}$$

where Ze is the hadron charge and $\delta n^{(h)}$ is the fluctuation of the hadron volume density. For MBEC, the latter quantity is assumed to be non-zero only within the limits of the modulator (thus, a relatively small kicker hadron feedback on the electron beam is typically neglected).

With these changes in mind, the previously-mentioned method of integration along unperturbed trajectories yields the following solution to the linearized, frequency-domain Vlasov equation:

$$\begin{aligned}&\delta\hat{F}_z(\mathbf{x},\mathbf{p},k_z,\eta;s) = \delta\hat{F}_z(\mathbf{x}_0,\mathbf{p}_0,k_z,\eta;0)\exp(-ik_z s\eta/\gamma_0^2) \\ &\times\exp(ik_z[\zeta_x(s)(p_x^2+x^2/\beta_x^2(s))/2+\zeta_y(s)(p_y^2+y^2/\beta_y^2(s))/2] - ik_z\sum_i R_{e,i}\eta H(s-s_{e,i})) \\ &- n_0\frac{e^2}{\gamma_0 m_e c^2}\frac{\partial F_0}{\partial\eta}\int_0^s ds'\Delta\hat{\mathcal{E}}_z(\mathbf{x}_+,k_z;s')\exp(ik_z[(s'-s)\eta/\gamma_0^2 - G_x(s,s')(p_x^2+x^2/\beta_x^2(s))/2 \\ &- G_y(s,s')(p_y^2+y^2/\beta_y^2(s))/2] + ik_z\sum_i R_{e,i}\eta[H(s'-s_{e,i})-H(s-s_{e,i})])\,. \end{aligned} \tag{35}$$

In the equation given above, $\zeta_{x,y}(s) \equiv \beta_{x,y}(s)\psi_{x,y}(s)$ and $G_{x,y}(s,s') \equiv \beta_{x,y}(s)(\psi_{x,y}(s') - \psi_{x,y}(s))$, where

$$\psi_{x,y}(s) = \int_0^s \frac{d\tilde{s}}{\beta_{x,y}(\tilde{s})} \tag{36}$$

are the betatron phase advance functions for the (idealized) electron lattice under consideration. Moreover, we have the definitions

$$\begin{aligned}\mathbf{x}_+ &= \mathbf{x}\sqrt{\beta_{x,y}(s')/\beta_{x,y}(s)}\cos(\Delta\psi_{x,y}(s,s')) + \sqrt{\beta_{x,y}(s)\beta_{x,y}(s')}\mathbf{p}\sin(\Delta\psi_{x,y}(s,s'))\,, \\ \mathbf{x}_0 &= \mathbf{x}\sqrt{\beta_{x,y}^{(0)}/\beta_{x,y}(s)}\cos(\psi_{x,y}(s)) - \sqrt{\beta_{x,y}^{(0)}\beta_{x,y}(s)}\mathbf{p}\sin(\psi_{x,y}(s))\,, \\ \mathbf{p}_0 &= \mathbf{x}\sin(\psi_{x,y}(s))/\sqrt{\beta_{x,y}^{(0)}\beta_{x,y}(s)} + \sqrt{\beta_{x,y}(s)/\beta_{x,y}^{(0)}}\mathbf{p}\cos(\psi_{x,y}(s))\,, \end{aligned} \tag{37}$$

where $\Delta\psi_{x,y}(s,s') \equiv \psi_{x,y}(s') - \psi_{x,y}(s)$ and $\beta_{x,y}^{(0)} \equiv \beta_{x,y}(s=0)$ are the initial values of the electron beta functions (or, equivalently, the electron betas in the modulator). Finally,

$\Delta\hat{\mathcal{E}}_z(\mathbf{x}, k_z; s) = \hat{\mathcal{E}}_z(\mathbf{x}, k_z; s) - Z\hat{\mathcal{E}}_z^{(h)}(\mathbf{x}, k_z; s)$, where $\hat{\mathcal{E}}_z^{(h)}$ is the Fourier component of the hadron space charge field, defined (in a manner completely analogous to its electron counterpart) by means of the relation

$$\mathcal{E}^{(h)}(\mathbf{x}, z; s) \equiv \int d^2\mathbf{x}' dz' \delta n^{(h)}(\mathbf{x}', z'; s)\Phi(\mathbf{x} - \mathbf{x}', z - z') = \frac{1}{2\pi}\int dk_z \hat{\mathcal{E}}_z^{(h)}(\mathbf{x}, k_z; s)\exp(ik_z z)\,. \tag{38}$$

Using the above results - and following the same procedure that led to Eqs. (29)-(30) - we ultimately obtain a general, self-consistent equation that describes the evolution of density fluctuations in the electron beam as the latter passes through the entire cooling lattice:

$$\begin{aligned}
\delta\hat{n}_{\mathbf{k}}(s) &= \delta\hat{n}_{\mathbf{k}}^{(0)}(s) + \frac{e^2 n_0 k_z^2}{\pi\gamma_0 m_e c^2}\int_0^s ds'((s'-s)/\gamma_0^2 + \sum_i R_{e,i}[H(s'-s_{e,i}) - H(s-s_{e,i})]) \\
&\times \frac{\exp(-\sigma_e^2 k_z^2((s'-s)/\gamma_0^2 + \sum_i R_{e,i}[H(s'-s_{e,i}) - H(s-s_{e,i})])^2/2)}{(1 + i\Sigma_x'^2(s)k_z G_x(s,s'))(1 + i\Sigma_y'^2(s)k_z G_y(s,s'))} \\
&\times \int d^2\mathbf{k}'_\perp \exp\left(-\frac{\Sigma_x^2(s)}{2}\frac{k_x^2 + (\beta_x(s')/\beta_x(s))k_x'^2 - 2(\beta_x(s')/\beta_x(s))^{1/2}k_x k_x'\cos(\Delta\psi_x(s,s'))}{1 + i\Sigma_x'^2(s)k_z G_x(s,s')}\right) \\
&\times \exp\left(-\frac{\Sigma_y^2(s)}{2}\frac{k_y^2 + (\beta_y(s')/\beta_y(s))k_y'^2 - 2(\beta_y(s')/\beta_y(s))^{1/2}k_y k_y'\cos(\Delta\psi_y(s,s'))}{1 + i\Sigma_y'^2(s)k_z G_y(s,s')}\right) \\
&\times \frac{\delta\hat{n}_{\mathbf{k}'_\perp, k_z}(s') - Z\delta\hat{n}^{(h)}_{\mathbf{k}'_\perp, k_z}(s')}{k_z^2 + \gamma_0^2\mathbf{k}_\perp'^2}\,,
\end{aligned} \tag{39}$$

where

$$\begin{aligned}
\delta\hat{n}_{\mathbf{k}}^{(0)}(s) = \int d^2\mathbf{x}d^2\mathbf{p}d\eta\delta\hat{F}_z(\mathbf{x}_0, \mathbf{p}_0, k_z, \eta; 0)\exp(-ik_z[s\eta/\gamma_0^2 - \zeta_x(s)(p_x^2 + x^2/\beta_x^2(s))/2 \\
- \zeta_y(s)(p_y^2 + y^2/\beta_y^2(s))/2] - ik_z\eta\sum_i R_{e,i}H(s - s_{e,i}) - i\mathbf{k}_\perp\cdot\mathbf{x})
\end{aligned} \tag{40}$$

and

$$\delta\hat{n}^{(h)}_{\mathbf{k}_\perp, k_z}(s) = \int d^2\mathbf{x}dz\exp(-i\mathbf{k}_\perp\cdot\mathbf{x} - ik_z z)\delta n^{(h)}(\mathbf{x}, z; s)\,. \tag{41}$$

We note that, apart from taking into account the betatron motion of the electrons, Eqs. (39)-(40) automatically include the effect of plasma oscillations in the e-beam for all the modules of the cooling system. For the special case with $\beta_x(s) = \beta_y(s) = \beta_p = 1/k_\beta$ and $\delta n^{(h)} = 0$, we have $\psi_{x,y}(s) = k_\beta s$, $\zeta_{x,y}(s) = s$ and $G_{x,y}(s,s') = s' - s$ and we indeed recover the original result (Eqs. (29)-(30)).

Turning to the kicker, we first point out that a crucial intermediate quantity that is of central importance in quantifying the performance of the cooler is the *generalized wake (or*

Greens function) $G(\mathbf{x}_k, \mathbf{x}_m, z_k - z_m)$ of the system, defined mathematically by means of the relation

$$\Delta\eta(\mathbf{x}_k, z_k) = \int d^2\mathbf{x}_m dz_m G(\mathbf{x}_k, \mathbf{x}_m, z_k - z_m)\delta n^{(h)}(\mathbf{x}_m, z_m)\,, \tag{42}$$

where $\Delta\eta(\mathbf{x}_k, z_k)$ is the total energy change of a kicker point hadron (at rest in the beam frame) in response to a hadron density fluctuation $\delta n^{(h)}(\mathbf{x}_m, z_m)$ in the modulator. To further clarify the physical meaning of the above definition, one can consider a single, point charge hadron fixed at $\mathbf{x} = \mathbf{x}_m\,, z = z_m$ inside a "sea" of (point) electrons in the modulator. Its presence creates a perturbation in the electron beam that can be propagated through the lattice. This perturbed e-beam acts back on a second point hadron in the kicker, located at $\mathbf{x} = \mathbf{x}_k\,, z = z_k$. The energy change of the second (kicker) hadron is expressed by $G(\mathbf{x}_k, \mathbf{x}_m, z_k - z_m)$. In a way, G can be viewed as a direct generalization of the conventional 1D wake, with the additional transverse position dependence arising as a result of the finite transverse extent of the electron beam.

Using the analytical machinery presented so far, it becomes conceptually straightforward to calculate the point hadron wake: for a single modulator hadron located at $z_m = 0$, one has $\delta n^{(h)}(\mathbf{x}, z; s) = \delta(\mathbf{x} - \mathbf{x}_m)\delta(z)$ so $\delta\hat{n}^{(h)}_{\mathbf{k}_\perp, k_z}(s) = \exp(-i\mathbf{k}_\perp \cdot \mathbf{x}_m)$. Using this input along with Eqs. (39)-(40) (and neglecting initial density modulations in the electron beam itself, i.e. assuming that $\delta\hat{F}_z(s = 0) = 0$) one can calculate the Fourier component $\delta\hat{n}_{\mathbf{k}_\perp, k_z}(\mathbf{x}_m, s)$ along the kicker (with $\mathbf{x}_m$ acting as an additional free parameter). Using Eq. (19), one can then obtain the equivalent field quantity $\hat{\mathcal{E}}_{\mathbf{k}_\perp, k_z}(\mathbf{x}_m, s)$, as well as its real space counterpart

$$\mathcal{E}(\mathbf{x}, z; \mathbf{x}_m, s) = (2\pi)^{-3} \int d^2\mathbf{k}_\perp dk_z \exp(i\mathbf{k}_\perp \cdot \mathbf{x} + ik_z z)\hat{\mathcal{E}}_{\mathbf{k}_\perp, k_z}(\mathbf{x}_m, s)\,. \tag{43}$$

As mentioned before, the generalized wake is obtained by considering the total energy change of the kicker hadron, i.e.

$$G(\mathbf{x}_k, \mathbf{x}_m, z_k) = \Delta\eta(\mathbf{x}_k, z_k) = -\frac{Ze^2}{\gamma_0 m_h c^2} \int_{L0}^{L0+L_k} ds\mathcal{E}(\mathbf{x}_k, z_k; \mathbf{x}_m, s)\,, \tag{44}$$

where m_h is the hadron mass and $s = L_0$ denotes the start of the kicker in the electron lattice. This procedure allows one to map the Green's function G for various hadron transverse position configurations.

III. NUMERICAL RESULTS

Having outlined the theoretical framework for calculating the generalized wake, we now turn to a simple numerical illustration that highlights the most important aspects of this topic. The parameters under consideration are listed in Table I and refer to a two-stage MBEC cooler for 100 GeV protons in the EIC. In Fig. 1 we show the comparison between theory and simulation as far the on-axis wake $w_0(z) = G(\mathbf{x}_k \to 0, \mathbf{x}_m \to 0, z)$ is concerned (i.e. for the case where both the modulator and the kicker proton have no transverse excursion. Here, as before, we also assume that $z_m = 0$ so that z represents the longitudinal position of the kicker proton). In particular, the theoretical wake is calculated using the methods of the previous section while the simulated wake is obtained by means of the macro-particle techniques discussed in our earlier EIC report ([1]). Two cases are considered, one for the peak value of the electron current ($I_e = 10$ A, left plot) and one for $I_e = 5$ A (right

TABLE I: Parameters for the generalized wake calculation

Case	**100 GeV**
Geometry	
Modulator Length (m)	33
Kicker Length (m)	33
Number of Amplifier Drifts	2
Amplifier Drift Lengths (m)	49
Electron Parameters	
Electron Peak Current (A)	~ 10
Electron Fractional Slice Energy Spread	1e-4
Electron Normalized Emittance (x/y) (mm-mrad)	2.8 / 2.8
Horizontal/Vertical Electron Betas in Modulator (m)	68 / 10
Horizontal/Vertical Electron Betas in Kicker (m)	30 / 4
Horizontal/ Vertical Electron Betas in Amplifiers (m)	12 / 12
R56 in First Electron Chicane (mm)	23
R56 in Second Electron Chicane (mm)	-17
R56 in Third Electron Chicane (mm)	-18

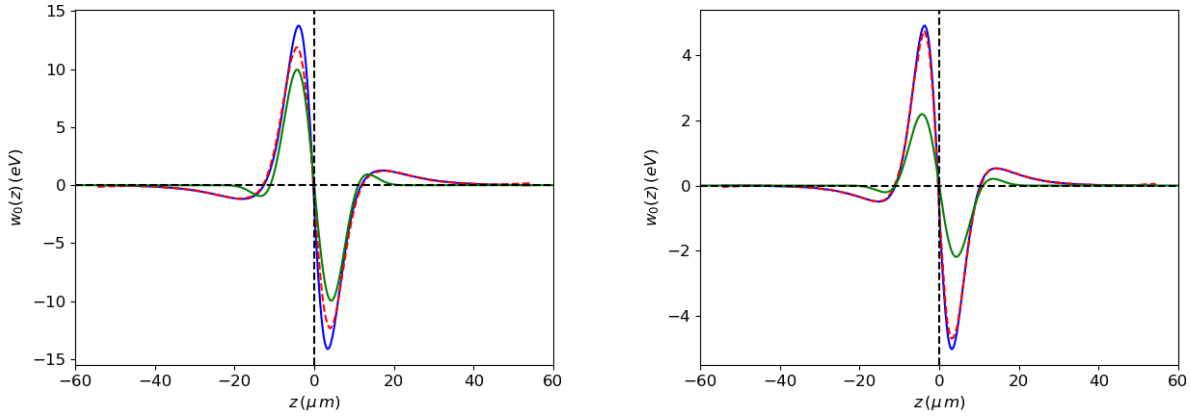

FIG. 1: On-axis wake profiles for the peak electron current (left) and half its peak value (right). Here, w_0 (which represents the total energy change of the kicker proton) is plotted versus the longitudinal position $z = z_k$ of the above-mentioned hadron, assuming $\mathbf{x}_k = 0$, $\mathbf{x}_m = 0$ and $z_m = 0$. Data shown are from 3D theory (blue solid lines), 3D simulation (red dashed lines) and the hybrid model (green solid lines). The hybrid model data are courtesy of W. Bergan.

plot). Moreover, for additional insight, our comparison includes data from a simplified, hybrid model in which the electrons are approximated by charged disks while the hadrons are treated as point charges [3]. It is worth noting that, up until our present analysis, such approximate models constituted the only available means for calculating the MBEC interaction wake [4–6]. In general, good agreement is observed between 3D theory and simulation, the small amplitude difference on the left plot likely being attributable to the gradual onset of nonlinear effects (saturation), which are expected to become more important the higher the electron beam current. Furthermore, compared to the hybrid model results, the 3D wakes roughly agree in terms of the overall shape of the profile (with the divergence being concentrated in the tails of the wake), while - in general - giving different estimates for the wake amplitude. As an empirical observation, this amplitude disagreement tends to get worse for lower current values.

Moving on from the purely on-axis case, Figs. 2-3 present the results of a study focusing on the dependence of the generalized wake upon the transverse position of the modulator and kicker ions. Specifically, Fig. 2 explores how the 3D theoretical wake profile changes when the kicker proton is moved to an off-axis position (with the modulator proton kept on-axis), while Fig. 3 modifies this scenario assuming an off-axis modulator proton and an

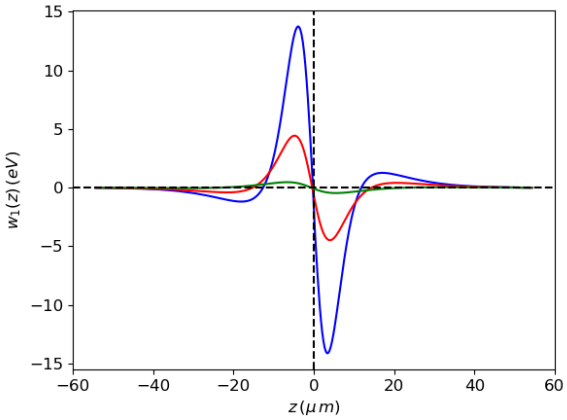

FIG. 2: Wake profiles for the peak electron current, an on-axis modulator proton ($x_m = y_m = 0$) and an off-axis kicker proton with various, fixed, transverse positions (so that $w_1(z) = G(\mathbf{x}_k \to \mathbf{x}_1, \mathbf{x}_m \to 0, z)$). The results shown here are from 3D theory alone, with $y_k = 0$ and $x_k/\sigma_{x,k} = x_1/\sigma_{x,k} = 0, 1.39, 2.78$ (blue/red/green curves, respectively).

on-axis kicker ion counterpart. In both cases, as expected, transverse excursion significantly diminishes the amplitude of the MBEC wake, as the off-axis protons sample a less intense part of the cooler electron beam (leading to an attenuated interaction overall). In fact, a more

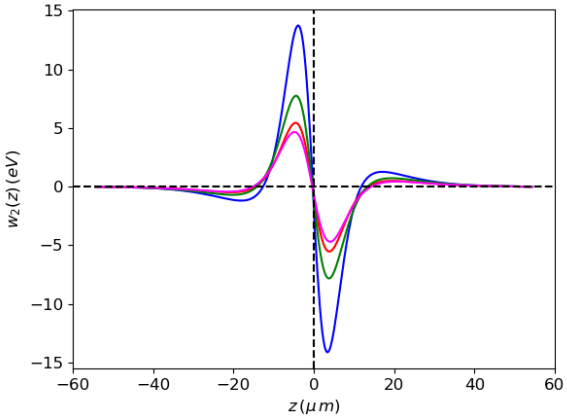

FIG. 3: Wake profiles for the peak electron current, an on-axis kicker proton ($x_k = y_k = 0$) and an off-axis modulator proton with various, fixed, transverse positions (so that $w_2(z) = G(\mathbf{x}_k \to 0, \mathbf{x}_m \to \mathbf{x}_2, z)$). As in Fig. 2, the results shown are from 3D theory alone, with $(x_2/\sigma_{x,m}, y_2/\sigma_{y,m}) = (0,0), (1.17,0), (0,1.17), (1,1)$ (blue/red/green/magenta curves, respectively).

detailed numerical study of the fully mapped generalized wake verifies that the maximum wake amplitude corresponds to the on-axis case. This allows one to quickly obtain a rough estimate of the difference in cooling performance between the fully 3D and hybrid models by simply comparing their respective on-axis wakes.

IV. CONCLUSIONS

In this note we have expanded on previous work in order to develop a rigorous, fully three-dimensional, theory-based technique for the study of microbunched electron cooling, including previously neglected effects such as the transverse motion of the electrons. A Vlasov equation-based, frequency-domain method has been used to track the modulation of the electron beam along the entire cooling lattice, allowing us to calculate and study the generalized wake of the cooler (a key figure of merit). Good agreement is observed between our theory and simulation-based approaches, and our results are - generally speaking - in line with those from approximate but computationally faster models, a fact which validates the performance estimates derived from the latter.

---

[1] P. Baxevanis, Tech. Rep. EIC-ADD-TN-021, BNL (2021).

[2] D. Ratner, Phys. Rev. Lett. **111**, 084802 (2013), URL `https://link.aps.org/doi/10.1103/PhysRevLett.111.084802`.

[3] W. F. Bergan and G. Stupakov, in *Proceedings of the 2022 NAPAC Conference, WEPA67* (Albuquerque, NM, USA, 2022).

[4] G. Stupakov, Phys. Rev. Accel. Beams **21**, 114402 (2018), URL `https://link.aps.org/doi/10.1103/PhysRevAccelBeams.21.114402`.

[5] G. Stupakov and P. Baxevanis, Phys. Rev. Accel. Beams **22**, 034401 (2019), URL `https://link.aps.org/doi/10.1103/PhysRevAccelBeams.22.034401`.

[6] P. Baxevanis and G. Stupakov, Phys. Rev. Accel. Beams **22**, 081003 (2019), URL `https://link.aps.org/doi/10.1103/PhysRevAccelBeams.22.081003`.